Synthesis of chitosan–iron keplerate composite as an adsorbent for removal of toxic ions from water

Saba Riad Khudhaier[a], Adil A. Awad[b], Dhafir T.A. Al-Heetimi[c],
Ahmed Jasim M. Al-Karawi[b,*], Emad M. Al-Kinani[b], Al-Ameen Bariz OmarAli[b],
Zyad Hussein J. Al-Qaisi[b], Qadoori Z. Khalaf[d]

[a]Department of Biology, College of Science, Mustansiriya University, Baghdad, Iraq, email: dr.sabariad@uomustansiriyah.edu.iq
[b]Department of Chemistry, College of Science, Mustansiriya University, P.O. Box 46010, Baghdad, Iraq,
emails: ahmedalkarawi@uomustansiriyah.edu.iq (A.J.M. Al-Karawi), adel80@uomustansiriyah.edu.iq (A.A. Awad),
emadmalek@uomustansiriyah.edu.iq (E.M. Al-Kinani), hero_802007@uomustansiriyah.edu.iq (A.-A.B. OmarAli),
zyadalqaisi@uomustansiriyah.edu.iq (Z.H.J. Al-Qaisi)
[c]Department of Chemistry, College of Education for Pure Science Ibn Al-Haitham, University of Baghdad, Baghdad, Iraq,
email: dhafir1973@gmail.com, dhafir.t.a@ihcoedu.uobaghdad.edu.iq
[d]College of Education, Al Iraqia University, Baghdad, Iraq, email: qadoorikhalaf1@yahoo.com

ABSTRACT

New composite: chitosan-iron keplerate (CHIK) as an adsorbent was prepared by the stirring of chitosan and iron keplerate at 40°C in acidic medium. This compound beside the free chitosan and iron keplerate were characterized using Fourier transform infrared spectroscopy (FTIR) and scanning electron microscopy techniques. Chitosan film (CH), iron keplerate (IK) and CHIK composite were used as adsorbents for the removal of Cu(II) and Cd(II) ions from water following the batch equilibrium method at pH = 5.5 (adsorption studies were performed with respect to contact time and adsorbent mass). The adsorption of metal ion on the surface of compounds was carried out by the aid of atomic absorption spectrophotometer. The adsorption studies displayed that the adsorption capacity of the free chitosan or free iron keplerate was enhanced upon the composition. The isothermal behavior together with the adsorption kinetics of metal ions on CHIK composite as a function of the temperature and the initial mass of CHIK were also studied. The two well-known isotherm models (Langmuir and Freundlich equations) were applied to fit the experimental data. The results show that the experimental data of the metal ion adsorption correlates well with the Langmuir isotherm equation.

Keywords: Chitosan; Iron Keplerate; Adsorption studies

1. Introduction

Removal of toxic metals from water has attracted remarkable interest because of the direct toxic effect of such metals to the main components of the environment (human beings, animals and plants). The most common toxic heavy metals in wastewater include: As, Pb, Hg, Cd, Cr, Cu, Ni, Ag and Zn. Release of heavy metals in high amounts into water creates serious problems for both of health and environment. And this may lead to an upsurge in wastewater treatment cost [1]. Nature and human are represent the main sources of heavy metals in wastewater. The natural factors involves volcanic activities, soil erosion, aerosols particulate

* Corresponding author.

and urban runoffs, while the human factors include mining extraction operations, metal finishing and electroplating processes, nuclear power and textile industries [2–7].

Chitosan (poly(D-glucosamine)) (Fig. 1a) represents one of the most naturally abundant biopolymers. This polymer particularly has fascinating properties (the most characteristic properties are the non-toxicity, biodegradability and biocompatibility). Furthermore, pure chitosan exhibits a good ability as an adsorbent for chemical or physical adsorption of metal ions. The relatively good capacity of chitosan to adsorb the metal ions can be attributed to the presence of amino and hydroxyl groups as good binding sites for cations. Due to these advantages, chitosan and its derivatives (Schiff bases, grafted copolymers, composites, nanoparticles, etc.) have many applications in drug release [8–17] (for more details regarding the application of chitosan and its derivatives in drug release, see review, [18] and references therein), biological activity [19–24] (for more details regarding the biological activity of chitosan and its derivatives, see review, [25] and references therein)), beverages and food industry [26–29] (also see [30] and references therein, an extensive review reporting the application of chitosan and its derivatives in beverages and food industry) as well as membranes for the removal of various pollutants such as metals, ions, dyes, pharmaceuticals/drugs, phenols, pesticides, herbicides, etc. [31–44] (references [31] and [44] are extensive reviews).

The variety of properties of spherical keplerates (porous polyoxometalates) of the type $\{(M)M_5\}_{12}$ (linker)$_{30}$ (M = Mo, W; linker = Fe^{3+}, Cr^{3+}, V^{IV} or $Mo_2^VO_4$) have animated research groups worldwide to design other related materials with unique properties. These materials are characteristic with gated pores and well-defined tunable internal and external surfaces either of the inorganic/hydrophilic or organic/hydrophobic type. In this context, fascinating chemical studies can be carried out at the outer and inner surfaces (for more details regarding the structure of such kind of clusters and their applications see references [45] and [46] and references therein).
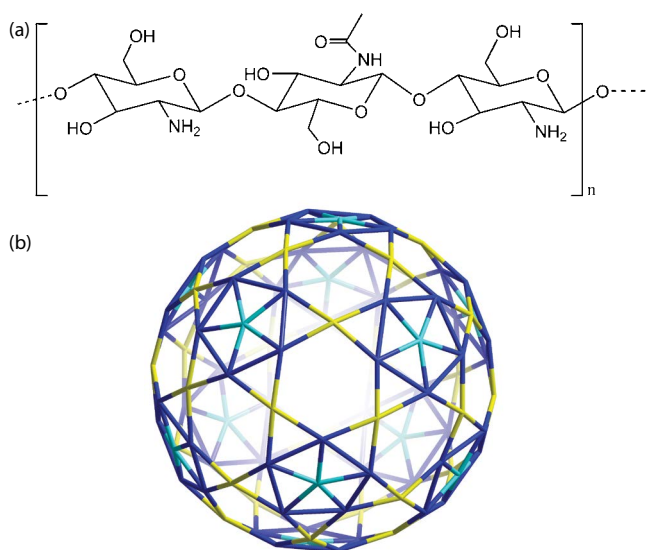
Iron keplerate ($\{Mo_{72}Fe_{30}\}$, Fig. 1b) is a discrete porous cluster which possesses a wide number of unique characteristics: (i) it displays a $\{Fe_{30}\}$ icosidodecahedron with 20 Fe_3–triangles and 20 $\{Fe_3Mo_6O_9\}$ pores with crown ether function [47], showing therefore unique magnetic properties [48,49]; (ii) self-assembles in dilute aqueous solution into single-layer membrane-like materials [50] as passive transporters for small cations [51]; (iii) it resembles a quasicrystal [52]; (iv) it is considered to be as a spherical analogue of the Kagomé lattices [53,54]. Accordingly, iron keplerate and other giant clusters have been the subject of numerous experimental and computational studies [45,48,49,55], including the study of their structures by X-ray single crystal spectroscopy and density functional theory (DFT) calculations [56]. Moreover, it is noteworthy that several $\{Mo_{72}Fe_{30}\}$-based composite materials have been designed for several applications, specifically in drug delivery [57,58] and in catalysis [59,60]. Generally, iron keplerate-type clusters have been prepared by treating the aqueous solution of the prototypal $\{Mo_{132}$–acetate$\}$ compound [61] with $FeCl_3$ [62,63]. But recently [64], it has been reported that the unprecedented self-assembly of $\{Mo_{72}Fe_{30}\}$-type clusters (as a yellow non-crystalline insoluble solid) can be directly formed from simple mixing of iron(III) chloride and sodium molybdate dihydrate in acidic medium.

In this paper, chitosan film (CH), iron keplerate (IK) and chitosan–iron keplerate (CHIK) composite are synthesized and characterized with IR and scanning electron microscopy (SEM). The adsorption of Cu(II) and Cd(II) onto prepared compounds (CH, IK and CHIK) based on the contact time, temperature and polymer mass, were investigated by the batch equilibrium method. The kinetics and isothermal behavior of the adsorption of metal ions on CHIK composite with respect to the initial mass of CHIK and temperature were also studied. Furthermore, the Langmuir and Freundlich isotherm models were used to fit the experimental data.

2. Experimental part

2.1. Materials

All reagents were commercially available and used without further purification. Iron(III) chloride hexahydrate (98%, Sigma-Aldrich Co., Germany); sodium molybdate dihydrate (≥99%, Sigma-Aldrich Co., Germany); high molecular weight chitosan (>75% deacetylated, Sigma-Aldrich Co., Germany), acetic acid (100%, Sigma-Aldrich Co., Germany); copper(II) chloride dihydrate (99.999%, Sigma-Aldrich Co., Germany); cadmium nitrate tetrahydrate (98%, Sigma-Aldrich Co., Germany).

2.2. Measurements

Elemental analysis for IK was obtained by using a 7300 V ICP-OES PerkinElmer-Optima Spectrometer (for Fe and Mo), (Germany) and by using a EuroEA 3000 Elemental Analyzer (for C and H). Infrared spectra (IR) were recorded on a 8400S-FT–IR Shimadzu spectrophotometer (ATR mode) and Raman spectrum for IK on a Raman Systems R3000HR spectrometer ($\lambda_{exc.}$ = 785 nm) (Germany). SEM micrographs were obtained using a JSM 6380LV-JEOL scanning electron microscope (Iraq). The micrographs were taken at 5,000× of

Fig. 1. Molecular structures of chitosan (a) and $\{Mo_{72}Fe_{30}\}$ cluster (IK) (b).

magnification. The samples were first sputtered with gold to obtain a layer of 150Å thickness using an Edwards S 150 Sputter Coater. Phoenix-986 AA spectrophotometer was used to obtain the atomic absorption data with wavelengths of 324.8 nm (for Cu) and 228.8 nm (for Cd). BS-11 thermostated shaker was used to shake and thermostat the samples.

2.3. Synthesis of compounds

2.3.1. Synthesis of chitosan film (CH)

A mixture of chitosan (1 g) and acetic acid (1%, 40 mL) was stirred at 40°C for 20 h. The yellow viscous solution was molded in a specific template to get a uniformed film of chitosan. Fourier transform infrared spectroscopy (FTIR) (υ/cm^{-1}): 3,600–3,100 (br., υ(OH) and υ(NH$_2$)); 2,918 (sh., υ_{as}(C–H)); 2,876 (w–m, υ_s(C–H)); 1,658 (m, υ(C=O) of the acetyl amide moiety); 1,645 (m, δ(NH)); 1,620 (m, υ(H$_2$O)); 1,593 (m); 1,465 (m, δ(C–H)); 1,382 (m); 1,322 (w); 1,155 (m); 1,076 (m); 1,032 (m); 707 (w); 614 (m); 463 (w).

2.3.2. Synthesis of iron keplerate (IK)

This compound was prepared according to the literature [64]. To a mixture of sodium molybdate dihydrate (3 g, 12.3 mmol), acetic acid (100%, 15 mL) and water (25 mL), iron(III) chloride hexahydrate (2.10 g, 7.7 mmol) was added (final pH ca. 2). The mixture was stirred vigorously for 30 min. The yellow precipitate was isolated by filtration, washed with water and dried in air. Yield: 2.2 g. Elemental analysis: Calculated for C$_{24}$H$_{528}$Fe$_{30}$Mo$_{78}$O$_{543}$ (M = 18,667 g mol^{-1}): C, 1.54; H, 2.85; Fe, 8.98; Mo, 40.09. Found: C, 1.61; H, 2.90; Fe, 8.63; Mo, 40.15. FTIR (υ/cm^{-1}): 1,620 (m, υ(H$_2$O)), 1,537 (m, υ_{as}(COO)), 1,412 (m, υ_s(COO)), 966 (m, υ(Mo=O)), 859 (m), 777 (s), 625 (m), 570 (s). Raman (solid state, $\lambda_{exc.}$ = 785 nm) (υ/cm^{-1}): 940 (vs), 905 (sh.), 832 (s), 706 (m), 508 (m), 429 (m), 361 (s), 246.

2.3.3. Synthesis of CHIK

Iron keplerate (IK) (0.15 g) was added to a mixture of chitosan (1 g) and acetic acid (1%, 40 mL). The mixture was stirred at 40°C for 48 h. The yellow viscous solution was molded in a specific template to get a uniformed film of chitosan–iron keplerate composite. FTIR (υ/cm^{-1}): 3,600–3,150 (br., υ(OH) and υ(NH$_2$)); 2,927 (sh., υ_{as}(C–H)); 2,854 (w–m, υ_s(C–H)); 1,657 (m, υ(C=O) of the acetyl amide moiety); 1,640 (m, δ(NH)); 1,618 (m, υ(H$_2$O)), 1,545 (m, υ_{as}(COO)), 1,468 (m, δ(C–H)); 1,427 (m, υ_s(COO)), 1,377 (m); 1,329 (w); 1,158 (m); 1,070 (m); 1,031 (m); 961 (m, υ(Mo=O)), 852 (m), 751 (s), 623 (m), 567 (s); 463 (w).

2.4. Adsorption studies

2.4.1. Adsorption of metal ions on the prepared compounds

The adsorption of metal ions (Cu(II) and Cd(II)) on the surface of the prepared compounds (IK, CH and CHIK) was carried out by the batch equilibrium method. 50 mL of aqueous solution of metal ion (100 ppm) was added to 0.1 g of dry compound (pH of the solution is 5.5), and the mixture was shaken at different temperatures (30°C, 40°C and 50°C) for specific period of time. The solid materials were removed

by filtration and the clear solution was measured by atomic absorption spectrophotometer (AAS) at λ = 324.8 nm for Cu and at λ = 228.8 nm for Cd, to determine the amount of metal ion remaining in solution. The effect of adsorbent mass on the adsorption of metal ions was carried out by using different masses of CHIK (0.15, 0.2 and 0.2.5 g) at 30°C.

2.4.2. Adsorption isotherms

The adsorption of metal ions (Cu(II) and Cd(II)) on the surface of the prepared compounds (IK, CH and CHIK) was carried out by the addition of 50 mL of aqueous solution of metal ions (100, 150, 200, 250 or 300 ppm) to 0.1 g of dry compound. The mixture was shaken at different temperatures: 30°C, 40°C and 50°C for the equilibrium time. The solid materials were removed by filtration and the clear solution was measured by AAS at λ = 324.8 nm for Cu and at λ = 228.8 nm for Cd, to determine the amount of metal ion remaining in solution.

2.4.3. Mathematical treatments

2.4.3.1. Mathematical equations of mass balance

In the isotherm experiments, the following mass balance equation was used to calculate the amount of metal ion (Cu(II) and Cd(II)) adsorbed at equilibrium, q_e (metal ion (mg)/adsorbent (g)):

$$q_e = \left(C_0 - C_e\right) \times \frac{V}{W} \tag{1}$$

C_0 (mg L^{-1}): the initial concentration of adsorbate; C_e (mg L^{-1}): the equilibrium concentration of the adsorbate; V (L): the volume of solution; W (g): the mass of dry adsorbent used.

While in the kinetic experiments, the amount of metal ion (Cu^{2+} or Cd^{2+}) adsorbed at any time, q_t (mg g^{-1}), was obtained from the following equation:

$$q_t = \left(C_0 - C_t\right) \times \frac{V}{W} \tag{2}$$

C_t (mg L^{-1}): the concentration of metal ion (Cu(II) and Cd(II)) in solution at any time t.

2.4.3.2. Isotherm models

Langmuir and Freundlich isotherms are well known to be as the most common adsorption models that usually used to fit the experimental data [65,66]. According to the Langmuir model, the equilibrium attained as soon a monolayer of the adsorbate molecules saturated the surface of the adsorbent. Eq. (3) shows the linear form of Langmuir model:

$$\frac{C_e}{q_e} = \left(\frac{1}{K_L q_{max}}\right) + \left(\frac{C_e}{q_{max}}\right) \tag{3}$$

q_{max}: Langmuir constant which related to the adsorption capacity; K_L: a constant related to the affinity between the adsorbate and the adsorbent.

The values of q_{max} and K_L can be obtained by plotting C_e/q_e vs. C_e. The value of q_e can be calculated by using Eq. (1). The dimensionless equilibrium parameter (R_L) can help in expressing the essential characteristics of the Langmuir isotherm [67]:

$$R_L = \frac{1}{\left(1 + K_L C_0\right)} \tag{4}$$

R_L value can give an indication for the type of the isotherm: $0 < R_L < 1$ (favorable), $R_L > 1$ (unfavorable), $R_L = 1$ (linear) or $R_L = 0$ (irreversible).

On the other hand, the Freundlich model is well known as one of the most important isotherms that expressed the multi-site adsorption isotherm for heterogeneous surfaces. This model presumes an initial surface adsorption followed by the condensation effect resulting from a strong solute–solute interaction. Eq. (5) displays the linear form of Freundlich isotherm.

$$\log q_e = \log K_F + \left(\frac{1}{n}\right) \log C_e \tag{5}$$

K_F is Freundlich constant which is related to maximum adsorption capacity, while n represents the exponent constant of Freundlich isotherm. This value gives an indication of how favorable the adsorption process is [68]. The values of K_F and n could be determined by plotting $\log q_e$ vs. $\log C_e$.

2.4.3.3. Kinetic models

Two kinetic models (pseudo-first-order and pseudo-second-order) are usually used to fit the experimental data. Eq. (6) shows the differential form of the pseudo-first-order kinetic model, while Eq. (7) displays the integral equation (boundary conditions, $t = 0$ to $t = t$ and $q_t = 0$ to $q_t = q_e$) [69]:

$$\frac{dq_t}{dt} = k_1 \left(q_e - q_t\right) \tag{6}$$

$$\ln\left(q_e - q_t\right) = -k_1 t + \ln q_e \tag{7}$$

k_1: the equilibrium rate constant of the pseudo-first-order (min^{-1}) and t is the time (min).

Plotting $\ln\left(q_e - q_t\right)$ vs. t of Eq. (7) gives a straight line (the slope of such straight line is $-k_1$, while the intercept is $\log q_e$).

Eq. (8) displays the differential form of the pseudo-first-order kinetic model, while Eq. (9) shows the integral equation (boundary conditions, $t = 0$ to $t = t$ and $q_t = 0$ to $q_t = q_e$) [70]:

$$\frac{dq_t}{dt} = k_2 \left(q_e - q_t\right)^2 \tag{8}$$

$$\frac{t}{q_t} = \frac{1}{k_2}\left(q_e\right)^2 + \frac{t}{q_e} \tag{9}$$

k_2: the equilibrium rate constant of the pseudo-second-order (g mg^{-1} h^{-1}); plotting t/q_t vs. t gives a straight line (the slope of the straight line is $1/q_e$, while the intercept is $1/k_2\,(q_e)^2$).

The thermodynamic parameters (the standard free energy: $\Delta G°$, the standard enthalpy: $\Delta H°$ and the standard entropy: $\Delta S°$) for the adsorption process were determined using Eq. (10) [70]:

$$\ln K_d = \left(\frac{\Delta S°}{R} - \frac{\Delta H°}{RT}\right) \tag{10}$$

R is universal gas constant (8.314 J mol^{-1} K^{-1}), T (K) is the temperature of absolute solution, whilst K_d is the distribution coefficient which could be obtained from Eq. (11):

$$K_d = \left(\frac{C_{Ae}}{C_e}\right) \tag{11}$$

C_{Ae} (mg L^{-1}): the amount of adsorbate that adsorbed on the surface of adsorbent at equilibrium; C_e (mg L^{-1}): the equilibrium concentration.

The standard enthalpy ($\Delta H°$) and the standard entropy ($\Delta S°$) can be determined by plotting $\ln K_d$ vs. $1/T$. The standard free energy ($\Delta G°$) was calculated by using the equation below:

$$\Delta G° = -RT \ln K_d \tag{12}$$

2.5. Desorption studies

0.1 g of IK, CH or CHIK was loaded with copper(II) using 50 mL of aqueous solution of copper(II) chloride dihydrate (100 ppm) at agitation period of 3 h. In order to remove any unadsorbed copper(II) ions, copper(II)-loaded IK, CH or CHIK was collected and washed thoroughly with distilled water. The amount of copper(II) adsorbed (mg) of IK, CH or CHIK was determined using the supernatant copper(II) concentration. IK, CH or CHIK were treated with 50 mL of EDTA of different concentration ($10^{-2} - 10^{-5}$ M) and the percentage of desorption of copper(II) was calculated by using the following equation:

$$\text{Desorption }(\%) = \left(\frac{m_r}{m_0}\right) \times 100\% \tag{13}$$

m_r (mg): the amount of copper(II) ions desorbed; m_0 (mg): the amount of copper(II) ions adsorbed.

3. Result and discussions

3.1. Synthesis and characterization of materials

The water insoluble iron keplerate (IK) was prepared by the simple mixing of metal salts (iron(III) chloride hexahydrate and sodium molybdate dihydrate) in acidic medium. While, CHIK composite was prepared by the stirring of chitosan (CH) and iron keplerate (IK) at 40°C in acidic medium.

The prepared compounds were characterized using different techniques. Iron keplerate was characterized by microelemental analysis, infrared (IR) and Raman spectroscopy in addition to SEM technique. While (CH) and

(CHIK) were characterized by IR spectroscopy and SEM. Microelemental analyses (C, H, Fe and Mo) data for IK were in a good agreement with the suggested formula (small deviation of molecular formula of iron keplerate between calculated and found is mainly due to the undefined water molecules outside the crystal lattice of the keplerate).

The FTIR spectra of the prepared compounds and the Raman spectrum of IK show characteristic bands consistent with the structures of these compounds (For more details see experimental part; and for examples see Fig. 2).

The surface morphology of the chitosan films (CH), iron keplerate (IK) and chitosan–iron keplerate composite (CHIK) was studied using SEM (the morphology of these compounds is reported in Fig. 3). The SEM micrographs for the CH and CHIK revealed that both films are plain, homogenous and nonporous textures. While the micrograph of IK is completely different, which shows the porous microcrystalline nature of the compound.

3.2. Adsorption studies

3.2.1. Rate of adsorption of metal ions

The adsorption of metal ions (Cu(II) and Cd(II)) by the prepared compounds (IK, CH and CHIK) was carried out by a batch equilibration technique as a function of contact time at pH = 5.5. The effect of agitation period on the adsorption of metal ions (Cu(II) and Cd(II)) by IK, CH and CHIK adsorbent is shown in Fig. 4. Results revealed that the amount of metal ions adsorbed (q_t) increases with time. Moreover, the rate of metal ions uptake decreases gradually with time
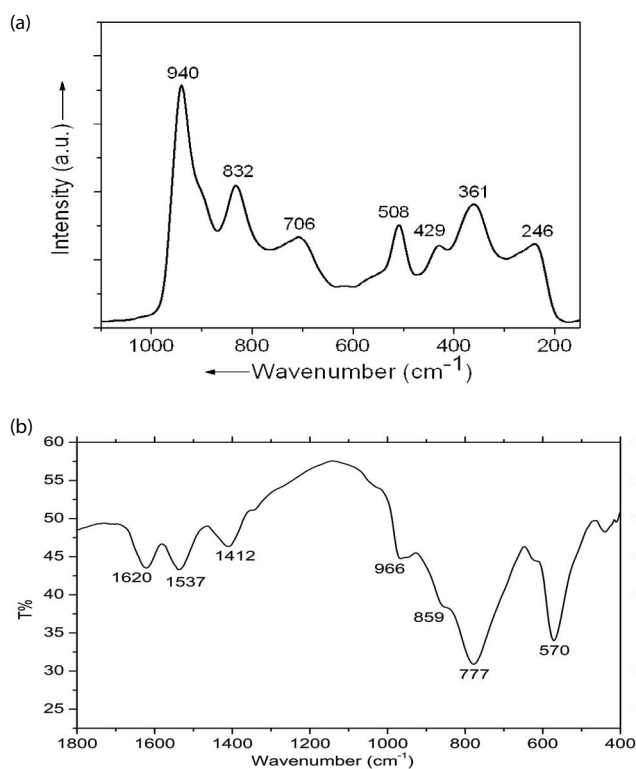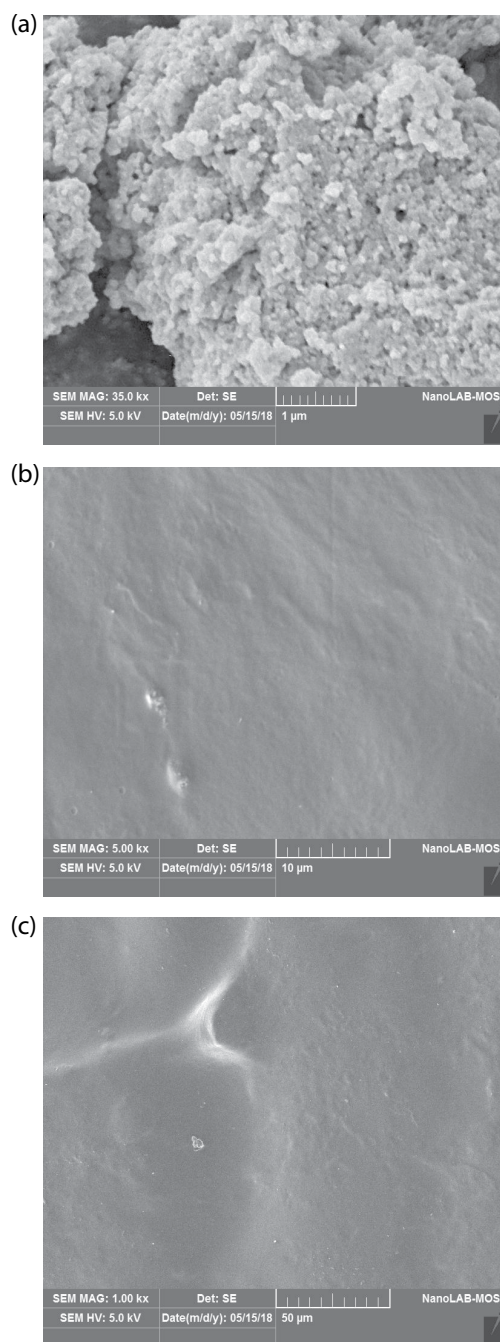
Fig. 2. Raman (a) and IR (b) spectra of IK.

Fig. 3. SEM micrographs of IK (a), CH (b) and CHIK (c).

until it reaches the value of pseudo-steady state value. This value is known as the equilibrium loading capacity (q_e). The equilibrium time of adsorption in all the three compounds (IK, CH and CHIK) was about 3 h. During the first hour of the adsorption process, the rate of adsorptions of metal ions sharply increased, then continues to increase but with a lower rate until approaches a steady state. These results demonstrate that the adsorption mechanism in the three compounds is similar in which the intraparticle diffusion played an important role in the adsorption process. 3 h (relatively short time) are needed to attain equilibrium. This revealed
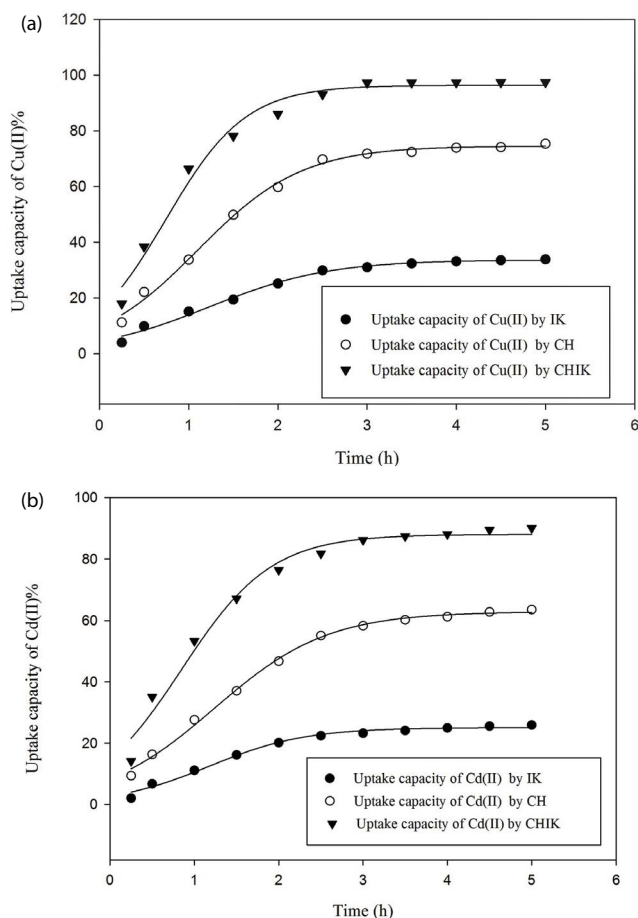
Fig. 4. Metal ions uptake (Cu²⁺ (a), Cd²⁺ (b)) by IK, CH and CHIK at 30°C as a function of contact time.

the negligible of the resistance of intraparticle diffusion. When equilibrium is settled, both of the metal ions in solution and metal ions adsorbed by the adsorbent would be in a state of dynamic equilibrium. This behavior suggests that further removal of metal ions is negligible and is mainly due to the continuous decrease in the concentration driving force and consequently elucidates the formation of a monolayer of metal ions on the external surface of the adsorbent [71].

The yellow powder of iron keplerate has the following properties which lead us to consider it as a good adsorbent: (i) insoluble in water even at high temperatures; (ii) has a spherical structure; (iii) the keplerate contains 20 crown ether type {Fe₃Mo₃O₆} pores and (iv) chemical studies can be carried out on the outer and inner surfaces as well as at the interface between the subunits of the keplerate. Furthermore, the previous studies showed that the pores of the keplerate have a specific size and this can be a host for ions with reasonable size [72–74].

On the other hand, chitosan as a natural insoluble polymer has been extensively investigated as an adsorbent for removal of organic dyes and heavy metals from water (mainly due to the presence of amino and hydroxyl groups, which can serve as the active sites).

It is notable that CHIK composite has a highest uptake capacity of metal ions, while IK has the lowest uptake

capacity (Fig. 4). This can be explained that the combining of IK and CH in a new composite significantly improved the capacity of interaction of both of pure IK and pure CH. Another notable that the percentage of copper(II) removed by CHIK is slightly higher than that of cadmium(II). This might be due to the difference in size between the copper(II) and cadmium(II) ions, and the defined size of the pores in iron keplerate (these pores are fixed to be as a host for ions with reasonable size [47,75,76]).

3.2.2. Effect of adsorbent mass on the adsorption of metal ions

The effect of CHIK mass on the adsorption of metal ions (Cu(II) and Cd(II)) was studied. Fig. 5 shows that the percentage of metal ion removed increases with the increasing of CHIK mass. This can be attributed to the increasing composite sites available for adsorption.

3.2.3. Adsorption isotherms

The significance of the adsorption isotherms generally gives an imagination about the distribution between the adsorbent and the solution at the equilibrium conditions. Furthermore, shows the effect of equilibrium concentration on the loading capacity of the adsorbate at different temperatures. Fig. 6 shows the adsorption of metal ions by CHIK at different temperatures (30°C, 40°C and 50°C). Results revealed that the adsorbent loading capacity increases with temperature. This behavior confirms the endothermic nature of the adsorption of metal ions onto CHIK.

Both of the Langmuir and Freundlich isotherm models were applied to fit the experimental data of the adsorption of metal ions by CHIK, Figs. S1 and S2, respectively. According to the correlation coefficient (R^2) values, the best fit of the experimental data was obtained from the Langmuir isotherm model (R^2 values of Langmuir isotherm model are higher than that of Freundlich isotherm model, Table 1). The results suggest that the adsorption of metal ions by CHIK is characterized by monolayer coverage of the metal ions on the outer surface of adsorbent. Moreover, the adsorption process has an equal activation energy or homogenous nature for each adsorbed molecule. On the other side, values of the separation factor (R_L) were in the range $0 < R_L < 1$, for the range of concentration of metal ions that was used in this study, which indicates that the adsorption of metal ions on CHIK
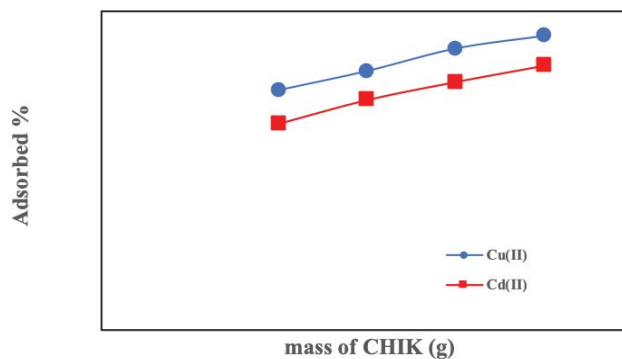

Fig. 5. Effect of CHIK mass on the percentage of the adsorbed Cu(II) and Cd(II).

particles is favorable. The mechanism of the adsorption of metal ions on porous adsorbents may involve the following steps: (i) diffusion of the metal ions to the external surface of adsorbent; (ii) diffusion of the metal ions into the pores of adsorbents; (iii) adsorption of the metal ions on the internal surface of adsorbent.

3.2.4. Adsorption kinetics

As previously mentioned, two major kinetic models (pseudo-first-order and pseudo-second-order) can be applied to fit the experimental data in order to examine the mechanism of the adsorption process. Fitting results of the experimental data are shown in Figs. 7 and 8 for the two models, respectively. While, the constants and correlation coefficient (R^2) for the two models are illustrated in Table 2. These figures display that the adsorption of metal ions by CHIK is best explained by the pseudo-second-order model. This is confirmed by the values of R^2 (Table 2). The kinetic model of the second-order presumes that the rate-limiting step may be chemical adsorption. It is more likely to predict that the adsorption behavior may involve valency forces
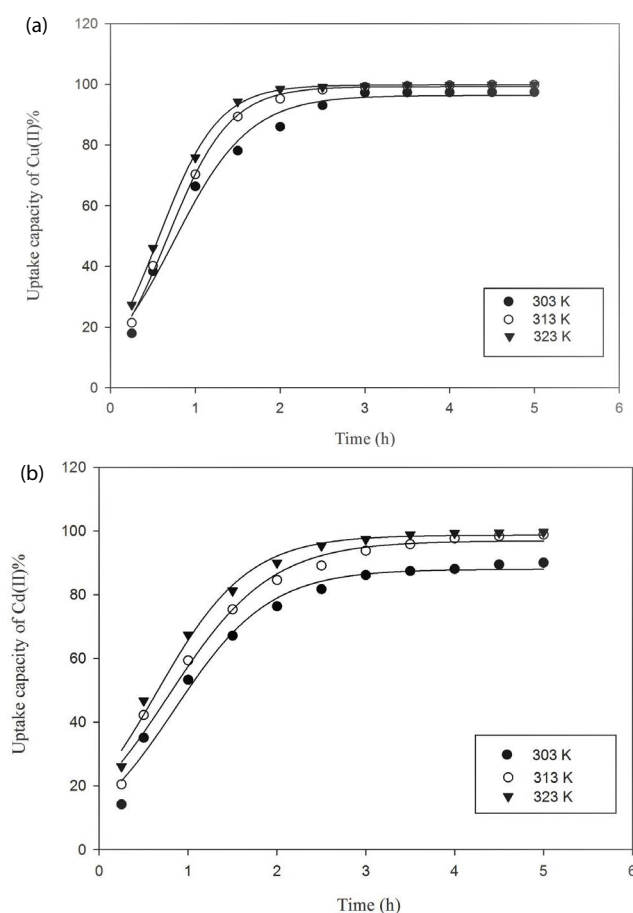

Fig. 6. Metal ions uptake (Cu^{2+} (a), Cd^{2+} (b)) by CHIK at different temperatures as a function of contact time.
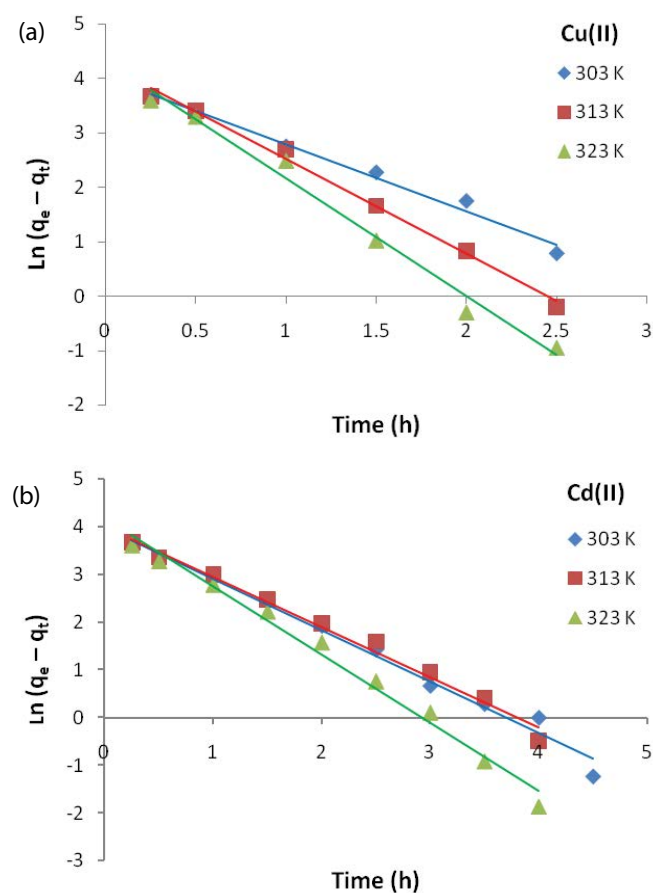

Fig. 7. Pseudo-first-order kinetics for adsorption of metal ions (Cu^{2+} (a), Cd^{2+} (b)) onto CHIK at different temperatures.

Table 1
Calculated values of Langmuir and Freundlich isothermal constants for the adsorption of metal ions by CHIK

Metal ion		Langmuir isotherm				Freundlich isotherm		
	T (K)	q_{max} (mg g^{-1})	K_L (L mg^{-1})	R^2		$1/n$	K_F (mg g^{-1})	R^2
Cu(II)	303	83.34	1.5	0.999		0.055	60.26	0.915
	313	90.91	1.22	0.999		0.048	67.14	0.688
	323	100	0.83	0.998		0.052	70.63	0.706
Cd(II)	303	76.92	1.38	0.999		0.087	48.64	0.536
	313	80.14	1.06	0.998		0.053	59.02	0.438
	323	83.34	0.71	0.999		0.060	61.66	0.547

through sharing of electrons between transition metal cations and adsorbent [66,70,77,78].

3.2.5. Adsorption thermodynamics

Almost all of the adsorption studies that reported earlier revealed in general that there is an increasing adsorption capacities of the adsorbent with temperature, which further proves that the nature of the adsorption of metal ions onto

Table 2
Comparison of the pseudo-first-order and pseudo-second-order models for the adsorption of metal ions by CHIK at 30°C (initial concentration of metal ions is 100 mg L^{-1})

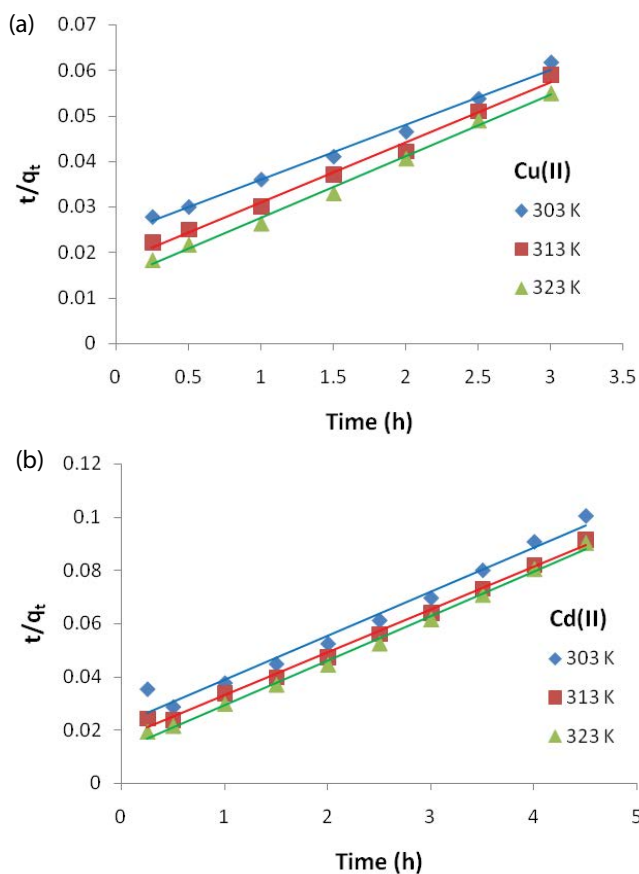| Adsorbate	T (K)	Pseudo-first-order model		Pseudo-second-order model	
		k_1 (h^{-1})	R^2	k_2 (g mg^{-1} h^{-1})	R^2
Cu(II)	303	1.227	0.987	0.0085	0.992
	313	1.735	0.982	0.0100	0.991
	323	2.158	0.985	0.0130	0.994
Cd(II)	303	1.073	0.986	0.0062	0.996
	313	1.122	0.988	0.0072	0.994
	323	1.426	0.987	0.0090	0.997

Fig. 8. Pseudo-second-order kinetics for adsorption of metal ions onto CHIK at different temperatures.

adsorbent is endothermic. This behavior established that there is increasing number of active surface centers that are available for adsorption, with temperature. Consequently, the viscosity of the liquid phase decreases, whilst the pore size increases; and ultimately enhancing the rate of intraparticle diffusion of solute molecules. The adsorption capacities of the composite (CHIK) that was prepared in this work have the same behavior (as the temperature increases, the adsorption capacities increases). Eqs. (10)–(12) were used to calculate the thermodynamic parameters ($\Delta H°$, $\Delta S°$, $\Delta G°$ and K_d) of the adsorption process. In order to accomplish these calculations, $\ln K_d$ was plotted against $1/T$ for CHIK as shown in Fig. 9. This figure displayed that the relationship between $\ln K_d$ and $1/T$ is linear (this further confirms the endothermic nature of the adsorption process). The correlation coefficient (R^2) with respect to the adsorption of Cd(II) ions ($R^2 = 0.9685$) seems to be much higher than that of Cu(II) ions ($R^2 = 0.8669$). Table 3 summarized the data of the thermodynamic parameters of the adsorption process for metal ions. The standard free energies ($\Delta G°$) for CHIK are negative and decrease as the temperature increases. The results show the feasibility and spontaneous nature of the process.

In addition, Table 3 exhibits positive values of $\Delta S°$ and $\Delta H°$ for CHIK, which was previously proved by the isotherm experiments at variable temperatures. The positive values of $\Delta S°$ display the affinity of the CHIK for adsorbates (Cu(II) or Cd(II) ions), as a result of the increased randomness at
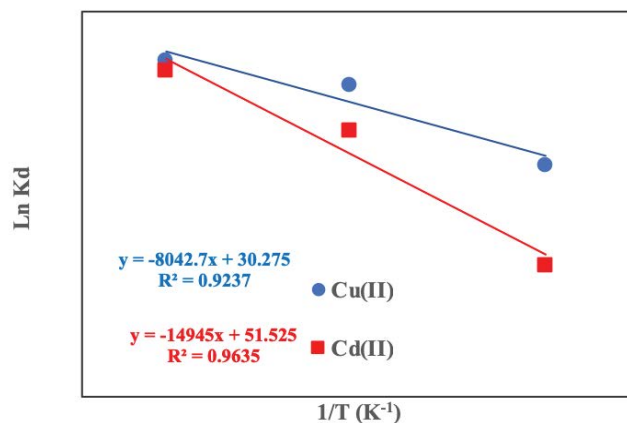

Fig. 9. Variation of thermodynamic parameters with temperature for the adsorption of metal ions on CHIK.

Table 3
Thermodynamic functions $\Delta G°$, $\Delta H°$ and $\Delta S°$, of Cu(II) and Cd(II) onto CHIK

Adsorbate	T (K)	$\Delta G°$ kJ mol^{-1}	$\Delta H°$ kJ mol^{-1}	$\Delta S°$ J mol^{-1} K^{-1}
Cu(II)	303	−9.059	66.861	251.66
	313	−12.628		
	323	−14.057		
Cd(II)	303	−5.123	124.252	428.34
	313	−10.718		
	323	−13.634		

Table 4
Some studies of the adsorption of metal/ions using modified chitosan as adsorbent during 2016–2018

Adsorbent	Metal/ions	Isotherms	q_{max} (mg g^{-1})	Reference
Zirconium–chitosan beads	B(III)	F	24.5	[32]
Chitosan–montmorillonite	Cu(II)	F	132.7	[33]
Chitosan-g-poly (acrylic acid)	Pb(II)	L	695.2	[34]
Chitosan-g-poly (acrylic acid)	Cd(II)	L	308.8	[34]
Chitosan/reduced graphene-oxide/ montmorillonite composite	Cr(VI)	L	87.03	[35]
Chitosan-g-poly (itaconic acid)	Pb(II)	L	1,320	[36]
Chitosan-g-poly (itaconic acid)	Hg(II)	L	870.1	[36]
Chitosan/poly(vinyl alcohol/CuO beads	Pb(II)	L	116.8	[37]
Chitosan/poly (vinyl alcohol) particles	ClO_4^-	L, F	28.15	[38]

Table 5
Percentage of desorption of Cu(II) from Cu–CH, Cu–IK and Cu–CHIK using EDTA solution

Compound	Concentration of EDTA (M)	Desorption (%)
Cu–CH	1.0×10^{-2}	–
	1.0×10^{-3}	–
	1.0×10^{-4}	51.70
	1.0×10^{-5}	32.11
Cu–IK	1.0×10^{-2}	88.13
	1.0×10^{-3}	74.46
	1.0×10^{-4}	63.83
	1.0×10^{-5}	46.33
Cu–CHIK	1.0×10^{-2}	85.93
	1.0×10^{-3}	70.25
	1.0×10^{-4}	59.14
	1.0×10^{-5}	41.46

the interface between the solid–liquid phases. These results can demonstrate a strategy for the adsorption of heavy metals such as Cu(II) or Cd(II) on the composite materials such as CHIK. Adsorption data of some previous studies of the adsorption of metal/ions using modified chitosan as adsorbent during 2016–2018 are listed in Table 4.

3.3. Desorption studies

The regeneration of adsorbents and the recovery of adsorbed material have become so important, especially in the recycling processes. Herein, the desorption studies are helpful in elucidating the nature of adsorption process and recovery of the metal ions from IK, CH and CHIK. Moreover, it also helps in the regeneration of these adsorbents, in order to be further used in the adsorption of metal ions. EDTA solution (with different concentrations) as a desorption agent was used to perform the desorption experiments. Both of the IK and CHIK adsorbents display good desorption results especially with the higher concentration of EDTA (chitosan is soluble at high concentration of EDTA solutions). EDTA

is well known as a hexadentate chelating agent and due to that, it is capable of forming a complex with copper(II) ions. The percentage of desorption of copper(II) ions from IK, CH and CHIK is depicted in Table 5.

4. Conclusions

Chitosan–iron keplerate (CHIK) composite was prepared via the stirring of chitosan and iron keplerate at 40°C in acidic medium. This compound beside the free chitosan and iron keplerate was characterized using FTIR and SEM techniques. SEM microgram shows that the CHIK film is plain, homogenous and nonporous texture. The prepared compounds (CH, IK and CHIK) are used as adsorbents for the removal of Cu(II) and Cd(II) ions from water following the batch equilibrium method at pH = 5.5. The adsorption studies were performed with respect to the time and adsorbent mass. The adsorption of metal ion on the surface of compounds was obtained by using AAS. These studies revealed that the adsorption capacity of the free chitosan or free iron keplerate was enhanced upon the composition. The isothermal behavior and the kinetic models of adsorption of metal ions on CHIK composite as a function of initial mass of CHIK and temperature were also studied. Based on the values of R^2, kinetic studies of the adsorption of metal ions (Cu(II) and Cd(II)) on CHIK is best described by the pseudo-second-order model. The experimental data of the adsorption of metal ions (Cu(II) and Cd(II)) were fitted with both of Langmuir and Freundlich isotherm models. The results show a good correlation of these data with the Langmuir isotherm equation.

References

[1] O.B. Akpor, G.O. Ohiobor, T.D. Olaolu, Heavy metal pollutants in wastewater effluents: sources, effects and remediation, Adv. Biosci. Bioeng., 2 (2014) 37–43.
[2] K. Sardar, S. Ali, S. Hameed, S. Afzal, S. Fatima, M.B. Shakoor, S.A. Bharwana, H.M. Tauqeer, Heavy metals contamination and what are the impacts on living organisms, Greener J. Environ. Manage. Public Saf., 2 (2013) 172–179.
[3] A. Amaral, J.V. Cruz, R.T. Cunha, A. Rodrigues, Baseline levels of metals in volcanic soils of the Azores (Portugal), Soil Sediment Contam., 15 (2006) 123–130.
[4] A.N. Kaizer, S.A. Osakwe, Physicochemical characteristics and heavy metal levels in water samples from five river systems in Delta State, Nigeria, J. Appl. Sci. Environ. Manage, 14 (2010) 83–87.

[5] A.M. Taiwo, A.O. Adeogun, K.A. Olatunde, K.O. Adegbite, Analysis of groundwater quality of hand-dug wells in peri-urban area of Obantoko, Abeokuta, Nigeria for selected physico-chemical parameters, Pac. J. Sci. Technol., 12 (2011) 527–534.

[6] E.K. Nguu, C.J. Mwita, P.M. Shiundu, D.O. Ogoyi, Determination of heavy metal content in water, sediment and microalgae from Lake Victoria, East Africa, Open Environ. Eng. J., 4 (2011) 156–161.

[7] W. Chaoyang, W. Cheng, Y. Linsheng, Characterizing spatial distribution and sources of heavy metals in the soils from mining-smelting activities in Shuikoushan, Hunan Province, China, J. Environ. Sci., 21 (2009) 1230–1236.

[8] X. Yu, Y. Mu, M. Xu, G. Xia, J. Wang, Y. Liu, X. Chen, Preparation and characterization of mucosal adhesive and two-step drug releasing cetirizine-chitosan nanoparticle, Carbohydr. Polym., 173 (2017) 600–609.

[9] S. Maity, P. Mukhopadhyay, P.P. Kundu, A.S. Chakraborti, Alginate coated chitosan core-shell nanoparticles for efficient oral delivery of naringenin in diabetic animals—an in vitro and in vivo approach, Carbohydr. Polym., 170 (2017) 124–132.

[10] S. Liu, S. Yang, P.C. Ho, Intranasal administration of carbamazepine-loaded carboxymethyl chitosan nanoparticles for drug delivery to the brain, Asian J. Pharm. Sci., 13 (2018) 72–81.

[11] S. Pistone, F.M. Goycoolea, A. Young, G. Smistad, M. Hiorth, Formulation of polysaccharide-based nanoparticles for local administration into the oral cavity, Eur. J. Pharm. Sci., 96 (2017) 381–389.

[12] B. Fonseca-Santos, M. Chorilli, An overview of carboxymethyl derivatives of chitosan: their use as biomaterials and drug delivery systems, Mater. Sci. Eng., C., 77 (2017) 1349–1362.

[13] J. Palacio, N.A. Agudelo, B.L. Lopez, PEGylation of PLA nanoparticles to improve mucus-penetration and colloidal stability for oral delivery systems, Curr. Opin. Chem. Eng., 11 (2016) 14–19.

[14] J. Wang, J. Tan, J. Luo, P. Huang, W. Zhou, L. Chen, L. Long, L.-M. Zhang, B. Zhu, L. Yang, D.Y. Deng, Enhancement of scutellarin oral delivery efficacy by vitamin B12-modified amphiphilic chitosan derivatives to treat type II diabetes induced-retinopathy, J. Nanobiotechnol., 15 (2017) 1–17.

[15] Y. Shi, L. Jia, Q. Du, J. Niu, D. Zhang, Surface-modified PLGA nanoparticles with chitosan for oral delivery of tolbutamide, Colloids Surf., B, 161 (2018) 67–72.

[16] L.A. Frank, P.S. Chaves, C.M. D'amore, R.V. Contri, A.G. Frank, R.C. Beck, A.R. Pohlmann, A. Buffon, S.S. Guterres, The use of chitosan as cationic coating or gel vehicle for polymeric nanocapsules: increasing penetration and adhesion of imiquimod in vaginal tissue, Eur. J. Pharm. Biopharm., 114 (2017) 202–212.

[17] A.J.M. Al-Karawi, Z.H.J. Al-Qaisi, A.H.J. Al-Qaisi, F.H.A. Al-Jeboori, Investigation of poly(methyl acrylate) grafted chitosan as a polymeric drug carrier, Polym. Bull., 71 (2014) 1575–1590.

[18] M.A. Mohammed, J. Syeda, K.M. Wasan, E.K. Wasan, An overview of chitosan nanoparticles and its application in non-parenteral drug delivery, Pharmaceutics, 9 (2017) 1–26.

[19] N.A. Mohamed, N.A. Abd El-Ghany, Synthesis, characterization, and antimicrobial activity of chitosan hydrazide derivative, Int. J. Polym. Mater. Polym. Biomater., 66 (2017) 410–415.

[20] L. Meng, X. Meng, R. Xing, S. Liu, X. Chen, Y. Qin, H. Yu, P. Li, Design, synthesis and antimicrobial activity of 6-*N*-substituted chitosan derivatives, Bioorg. Med. Chem. Lett., 26 (2016) 4548–4551.

[21] H.D. Follmann, A.F. Martins, T.M. Nobre, J.D. Bresolin, T.S. Cellet, P. Valderrama, D.S. Correa, E.C. Muniz, O.N. Oliveira Jr., Extent of shielding by counterions determines the bactericidal activity of *N,N,N*-trimethyl chitosan salts, Carbohydr. Polym., 137 (2016) 418–425.

[22] S.A. Loutfy, H.M.A. El-Din, M.H. Elberry, N.G. Allam, M.T.M. Hasanin, A.M. Abdellah, Synthesis, characterization and cytotoxic evaluation of chitosan nanoparticles: *in vitro* liver cancer model, Adv. Nat. Sci.: Nanosci. Nanotechnol., 7 (2016) 035008.

[23] O. Zaki, S. Sarah, M.N. Ibrahim, H. Katas, Particle size affects concentration-dependent cytotoxicity of chitosan nanoparticles towards mouse hematopoietic stem cells, J. Nanotechnol., 2015 (2015) 1–5.

[24] M. Hosseinnejad, S.M. Jafari, Evaluation of different factors affecting antimicrobial properties of chitosan, Int. J. Biol. Macromol., 85 (2016) 467–475.

[25] P. Sahariah, M. Masson, Antimicrobial chitosan and chitosan derivatives: a review of the structure–activity relationship, Biomacromolecules,18 (2017) 3846–3868.

[26] M.J. Valera, F. Sainz, A. Mas, M.J. Torija, Effect of chitosan and SO$_2$ on viability of Acetobacter strains in wine, Int. J. Food Microbiol., 246 (2017) 1–4.

[27] B. He, J. Ge, P. Yue, X. Yue, R. Fu, J. Liang, X. Gao, Loading of anthocyanins on chitosan nanoparticles influences anthocyanin degradation in gastrointestinal fluids and stability in a beverage, Food Chem., 221 (2017) 1671–1677.

[28] V. Ghormade, E.K. Pathan, M.V. Deshpande, Can fungi compete with marine sources for chitosan production?, Int. J. Biol. Macromol., 104 (2017) 1415–1421.

[29] A. Zimoch-Korzycka, C. Gardrat, M. Al Kharboutly, A. Castellan, I. Pianet, A. Jarmoluk, V. Coma, Chemical characterization, antioxidant and anti-listerial activity of non-animal chitosan-glucan complexes, Food Hydrocolloids, 61 (2016) 338–343.

[30] M.A.M. Rocha, M.A. Coimbra, C. Nunes, Applications of chitosan and their derivatives in beverages: a critical review, Curr. Opin. Food Sci., 15 (2017) 61–69.

[31] R. Yang, H. Li, M. Huang, H. Yang, A. Li, A review on chitosan-based flocculants and their applications in water treatment, Water Res., 95 (2016) 59–89.

[32] J. Kluczka, M. Gnus, A. Kazek-Kęsik, G. Dudek, Zirconium-chitosan hydrogel beads for removal of boron from aqueous solutions, Polymer, 150 (2018) 109–118.

[33] F.A. Ngwabebhoh, A. Erdem, U. Yildiz, Synergistic removal of Cu(II) and nitrazine yellow dye using an eco-friendly chitosan-montmorillonite hydrogel: optimization by response surface methodology, J. Appl. Polym. Sci., 133 (2016) 43664–43678.

[34] Y. Zhu, Y. Zheng, F. Wang, A. Wang, Fabrication of magnetic macroporous chitosan-*g*-poly (acrylic acid) hydrogel for removal of Cd^{2+} and Pb^{2+}, Int. J. Biol. Macromol., 93 (2016) 483–492.

[35] P. Yu, H.-Q. Wang, R.-Y. Bao, Z. Liu, W. Yang, B.-H. Xie, M.-B. Yang, Self-assembled sponge-like chitosan/reduced graphene oxide/montmorillonite composite hydrogels without cross-linking of chitosan for effective Cr(VI) sorption, ACS Sustainable Chem. Eng., 5 (2017) 1557–1566.

[36] H. Ge, T. Hua, J. Wang, Preparation and characterization of poly (itaconic acid)-grafted crosslinked chitosan nanoadsorbent for high uptake of Hg^{2+} and Pb^{2+}, Int. J. Biol. Macromol., 95 (2017) 954–961.

[37] X. Jiao, Y. Gutha, W. Zhang, Application of chitosan/poly(vinyl alcohol)/CuO (CS/PVA/CuO) beads as an adsorbent material for the removal of Pb(II) from aqueous environment, Colloids Surf., B, 149 (2017) 184–195.

[38] Y.-H. Xie, Y.-L. Wu, Y.-H. Qin, Y. Yi, Z. Liu, L. Lv, M. Xu, Evaluation of perchlorate removal from aqueous solution by cross-linked magnetic chitosan/poly (vinyl alcohol) particles, J. Taiwan Inst. Chem. Eng., 65 (2016) 295–303.

[39] T.V. Charpentier, A. Neville, J.L. Lanigan, R. Barker, M.J. Smith, T. Richardson, Preparation of magnetic carboxymethylchitosan nanoparticles for adsorption of heavy metal ions, ACS Omega, 1 (2016) 77–83.

[40] Y. Fu, Y. Huang, J. Hu, Preparation of chitosan/MCM-41-PAA nanocomposites and the adsorption behaviour of Hg(II) ions, R. Soc. Open Sci., 5 (2018) 171927.

[41] R. Bazargan-Lari, H.R. Zafarani, M.E. Bahrololoom, A. Nemati, Removal of Cu(II) ions from aqueous solutions by low-cost natural hydroxyapatite/chitosan composite: equilibrium, kinetic and thermodynamic studies, J. Taiwan Inst. Chem. Eng., 45 (2014) 1642–1648.

[42] R. Bazargan-Lari, M.E. Bahrololoom, A. Nemati, Sorption behavior of Zn (II) ions by low cost and biological natural hydroxyapatite/chitosan composite from industrial waste water, J. Food Agric. Environ., 9 (2011) 892–897.

[43] A.J.M. Al-Karawi, Z.H.J. Al-Qaisi, H.I. Abdullah, A.M.A. Al-Mokaram, D.T.A. Al-Heetimi, Synthesis, characterization of acrylamide grafted chitosan and its use in removal of copper(II) ions from water, Carbohydr. Polym., 83 (2011) 495–500.

[44] W.W. Ngah, L. Teong, M. Hanafiah, Adsorption of dyes and heavy metal ions by chitosan composites: a review, Carbohydr. Polym., 83 (2011) 1446–1456.

[45] A. Müller, P. Gouzerh, From linking of metal-oxide building blocks in a dynamic library to giant clusters with unique properties and towards adaptive chemistry, Chem. Soc. Rev., 41 (2012) 7431–7463.

[46] L. Cronin, A. Müller, From serendipity to design of polyoxometalates at the nanoscale, aesthetic beauty and applications, Chem. Soc. Rev., 41 (2012) 7333–7334.

[47] A.M. Todea, A. Merca, H. Bögge, T. Glaser, J.M. Pigga, M.L. Langston, T. Liu, R. Prozorov, M. Luban, C. Schröder, Porous capsules $\{(M)M_5\}_{12}Fe_{30}^{III}$ (M=Mo^{VI}, W^{VI}): sphere surface supramolecular chemistry with 20 ammonium ions, related solution properties, and tuning of magnetic exchange interactions, Angew. Chem. Int. ed., 49 (2010) 514–519.

[48] P. Koegerler, B. Tsukerblat, A. Mueller, Structure-related frustrated magnetism of nanosized polyoxometalates: aesthetics and properties in harmony, Dalton Trans., 39 (2010) 21–36.

[49] D. Gatteschi, R. Sessoli, J. Villain, Molecular Nanomagnets, Oxford University Press, Oxford, 2006.

[50] T. Liu, B. Imber, E. Diemann, G. Liu, K. Cokleski, H. Li, Z. Chen, A. Mueller, Deprotonations and charges of well-defined $\{Mo_{72}Fe_{30}\}$ nanoacids simply stepwise tuned by pH allow control/variation of related self-assembly processes, J. Am. Chem. Soc., 128 (2006) 15914–15920.

[51] P.P. Mishra, J. Pigga, T. Liu, Membranes based on "Keplerate"-type polyoxometalates: Slow, passive cation transportation and creation of water microenvironment, J. Am. Chem. Soc., 130 (2008) 1548–1549.

[52] A. Müller, Predicting a structured future, Nat. Chem., 1 (2009) 13–14.

[53] I. Rousochatzakis, A.M. Laeuchli, F. Mila, Highly frustrated magnetic clusters: the kagomé on a sphere, Phys. Rev. B: Condens. Matter, 77 (2008) 094420.

[54] S.K. Pati, C. Rao, Kagome network compounds and their novel magnetic properties, Chem. Commun., 39 (2008) 4683–4693.

[55] L. Engelhardt, C. Schröder, Simulating Computationally Complex Magnetic Molecules, R. Winpenny, Molecular Cluster Magnets, World Scientific, Singapore, 2012, pp. 241–296.

[56] K. Kuepper, C. Derks, C. Taubitz, M. Prinz, L. Joly, J.-P. Kappler, A. Postnikov, W. Yang, T.V. Kuznetsova, U. Wiedwald, P. Ziemann, M. Neumann, Electronic structure and soft-X-ray-induced photoreduction studies of iron-based magnetic polyoxometalates of type $\{(M)M_5\}_{12}Fe_{30}^{III}$ (M = Mo^{VI}, W^{VI}), Dalton Trans., 42 (2013) 7924–7935.

[57] J. Cui, D. Fan, J. Hao, Magnetic $\{Mo_{72}Fe_{30}\}$-embedded hybrid nanocapsules, J. Colloid Interface Sci., 330 (2009) 488–492.

[58] D. Fan, J. Hao, Magnetic aligned vesicles, J. Colloid Interface Sci., 342 (2010) 43–48.

[59] S. Roy, H.J. Meeldijk, A.V. Petukhov, M. Versluijs, F. Soulimani, Synthesis and characterization of $\{Mo_{72}Fe_{30}\}$-coated large hexagonal gibbsite γ-Al(OH)$_3$ platelets, Dalton Trans., 21 (2008) 2861–2865.

[60] D. Fan, J. Hao, Fabrication and electrocatalytic properties of chitosan and Keplerate-type polyoxometalate $\{Mo_{72}Fe_{30}\}$ hybrid films, J. Phys. Chem. B., 113 (2009) 7513–7516.

[61] A. Müller, E. Krickemeyer, H. Bögge, M. Schmidtmann, F. Peters, Organizational forms of matter: an inorganic super fullerene and keplerate based on molybdenum oxide, Angew. Chem. Int. ed., 37 (1998) 3359–3363.

[62] A. Müller, S. Sarkar, S.Q.N. Shah, H. Bögge, M. Schmidtmann, S. Sarkar, P. Kögerler, B. Hauptfleisch, A.X. Trautwein, V. Schünemann, Archimedean synthesis and magic numbers: "sizing" giant molybdenum-oxide-based molecular spheres of the keplerate type, Angew. Chem. Int. ed., 38 (1999) 3238–3241.

[63] A. Müller, S.K. Das, E. Krickemeyer, P. Kögerler, H. Bögge, M. Schmidtmann, Cross-linking nanostructured spherical capsules as building units by crystal engineering: related chemistry, Solid State Sci., 2 (2000) 847–854.

[64] K. Kuepper, M. Neumann, A.J.M. Al-Karawi, A. Ghosh, S. Walleck, T. Glaser, P. Gouzerh, A. Müller, Immediate formation/precipitation of icosahedrally structured iron–molybdenum mixed oxides from solutions upon mixing simple iron(III) and molybdate salts, J. Cluster Sci., 25 (2014) 301–311.

[65] I. Tan, B. Hameed, A. Ahmad, Equilibrium and kinetic studies on basic dye adsorption by oil palm fibre activated carbon, Chem. Eng. J., 127 (2007) 111–119.

[66] H.M. Zalloum, Z. Al-Qodah, M.S. Mubarak, Copper adsorption on chitosan-derived Schiff bases, J. Macromol. Sci. Part A Pure Appl. Chem., 46 (2008) 46–57.

[67] T.W. Weber, R.K. Chakravorti, Pore and solid diffusion models for fixed-bed adsorbers, AIChE J., 20 (1974) 228–238.

[68] M. Hosseini, S.F. Mertens, M. Ghorbani, M.R. Arshadi, Asymmetrical Schiff bases as inhibitors of mild steel corrosion in sulphuric acid media, Mater. Chem. Phys., 78 (2003) 800–808.

[69] J. Igwe, A. Abia, Adsorption isotherm studies of Cd(II), Pb(II) and Zn(II) ions bioremediation from aqueous solution using unmodified and EDTA-modified maize cob, Eclética Quím., 32 (2007) 33–42.

[70] Y.S. Ho, G. McKay, Sorption of dye from aqueous solution by peat, Chem. Eng. J., 70 (1998) 115–124.

[71] M. Al-Ghouti, M. Khraisheh, S. Allen, M. Ahmad, The removal of dyes from textile wastewater: a study of the physical characteristics and adsorption mechanisms of diatomaceous earth, J. Environ. Manage, 69 (2003) 229–238.

[72] A.M. Todea, A.J.M. Al-Karawi, T. Glaser, S. Walleck, L.-M. Chamoreau, R. Thouvenot, P. Gouzerh, A. Müller, Encapsulation of Keggin-type anions in reduced molybdenum–iron-type Keplerates as a general phenomenon, Inorg. Chim. Acta, 389 (2012) 107–111.

[73] A.M. Todea, J. Szakács, S. Konar, H. Bögge, D.C. Crans, T. Glaser, H. Rousselière, R. Thouvenot, P. Gouzerh, A. Müller, Reduced molybdenum-oxide-based core-shell hybrids: "blue" electrons are delocalized on the shell, Chem. Eur. J., 17 (2011) 6635–6642.

[74] A. Müller, S.K. Das, P. Kögerler, H. Bögge, M. Schmidtmann, A.X. Trautwein, V. Schünemann, E. Krickemeyer, W. Preetz, A new type of supramolecular compound: molybdenum-oxide-based composites consisting of magnetic nanocapsules with encapsulated keggin-ion electron reservoirs cross-linked to a two-dimensional network, Angew. Chem. Int. ed., 39 (2000) 3413–3417.

[75] A. Müller, F.L. Sousa, A. Merca, H. Bögge, P. Miró, J.A. Fernandez, J.M. Poblet, C. Bo, Supramolecular chemistry on a cluster surface: fixation/complexation of potassium and ammonium ions with crown-ether-like rings, Angew. Chem. Int. ed., 48 (2009) 5934–5937.

[76] A. Müller, A. Merca, A.J.M. Al-Karawi, S. Garai, H. Bögge, G. Hou, L. Wu, E.T. Haupt, D. Rehder, F. Haso, Chemical adaptability: the integration of different kinds of matter into giant molecular metal oxides, Chem. Eur. J., 18 (2012) 16310–16318.

[77] W.W. Ngah, A. Kamari, Y. Koay, Equilibrium and kinetics studies of adsorption of copper (II) on chitosan and chitosan/PVA beads, Int. J. Biol. Macromol., 34 (2004) 155–161.

[78] K.C. Justi, M.C. Laranjeira, A. Neves, A.S. Mangrich, V.T. Fávere, Chitosan functionalized with 2[-bis-(pyridylmethyl) aminomethyl]4-methyl-6-formyl-phenol: equilibrium and kinetics of copper (II) adsorption, Polymer, 45 (2004) 6285–6290.
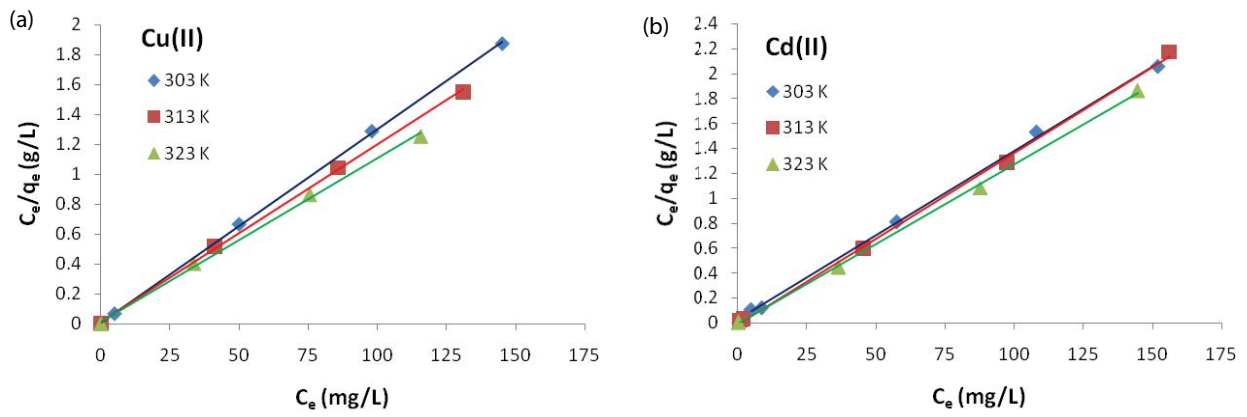
Supplementary Information

Fig. S1. Linearized Langmuir for metal ions adsorption (Cu^{2+} (a), Cd^{2+} (b)) by CHIK at different temperatures.
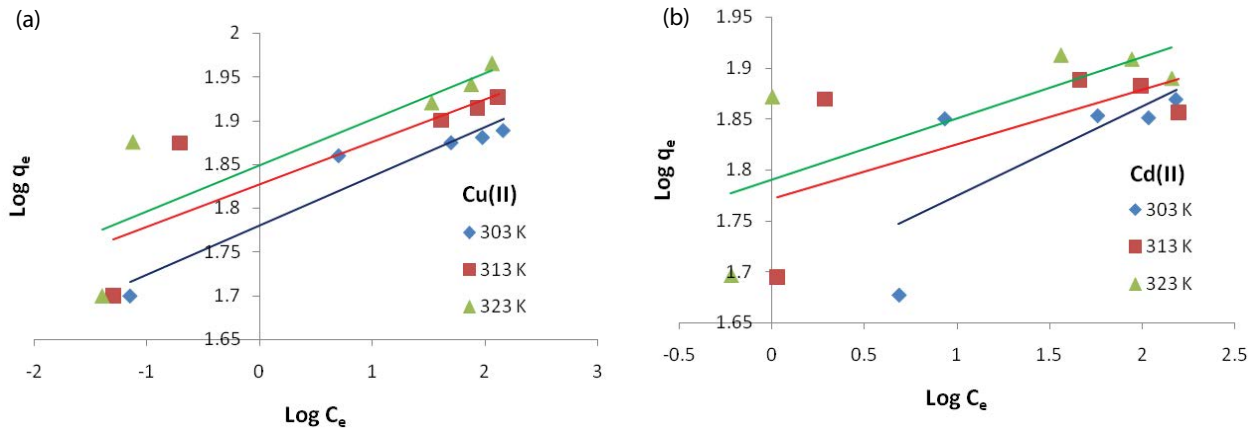

Fig. S2. Linearized Freundlich for metal ions adsorption (Cu^{2+} (a), Cd^{2+} (b)) by CHIK at different temperatures.